Aero-optical Foundations and Applications

George W. Sutton
Helionetics Inc., San Diego, California

Nomenclature

A = coefficient defined in Eq. (A40)
A_0 = area
$\boldsymbol{B}$ = magnetic field
c = speed of light
C = correlation function
C_n = index of refraction structure function constant
C_p = specific heat
D = diameter of aperture
$\boldsymbol{D}$ = electric displacement
E = spectrum
$\boldsymbol{E}$ = electric field
$\boldsymbol{H}$ = magnetic induction
I = intensity
J_i = Bessel function of order i
k = wave number
l = turbulence scale size
L = path length
m = exponent
M = Mach number
n = index of refraction; exponent
p = pressure
P = power
P_i = Legendre polynomial
r = radius
r_0 = aperture coherence length
R = range
t = time
T = temperature
u = electric field
v = speed
V = volume
x,y,z = rectangular coordinates
α = extinction coefficient
γ = ratio of specific heats
Δ = rms
δ = boundary-layer thickness
ϵ_0 = turbulent thermal diffusivity
θ = scattering angle
κ = permittivity
Λ = integral scale size
λ = wavelength
μ = permeability
ξ,η,ζ = Cartesian dummy coordinates
ρ = density
ρ,θ,ϕ = spherical coordinates
σ = scattering cross section, standard deviation
Φ = phase

I. Introduction

IN the past, optical diagnostics such as schlieren, shadowgraphs, and interferometry have been used to analyze aerodynamic flow experimentally through the dependence of the index of refraction on gas density; more recently holography has been used. On the other hand, density inhomogeneities in the flowfield can perturb other optical phenomena, namely, the ability to image or propagate laser beams through the flowfield. In general, the inhomogeneities can be classified as steady, unsteady, and random. The state-of-the-art of aero-optical phenomena in 1982 can best be summarized by contrasting two quotations from the same symposium:

> By 1980 it was apparent that aero-optics flight testing had reached an apex and further extensive flight measurements were not required.[1]
>
> There is clearly no simple rule-of-thumb answer to estimating the degradation in a light beam propagated through the aerodynamic boundary layer of an aircraft.[2]

A possible reconciliation of the above statements is that the latter is due to aerodynamic effects whose parameters are not yet known; the former statement could mean that additional flight testing alone would not reveal the nature of the unknown parameters. This paper will attempt to indicate

---

Dr. Sutton received his BME with honors from Cornell University, then his MSME and Ph.D. (magna cum laude) in mechanical engineering and physics from California Institute of Technology. He has undertaken additional studies in fluid mechanics, turbulence, magnetohydrodynamics, plasma physics, and supersonic aerodynamics at the University of Pennsylvania. He is currently manager of government program development at the Helionetics Laser Division, where he is also active in the analysis and design of Raman wavelength conversion gas cells for excimer lasers. At Avco Everett Research Laboratory, Inc., Dr. Sutton was Vice President for government laser development programs and was responsible for the engineering development of complete laser systems. Before that he was director of strategic technology programs, which included all AERL research, development, and field programs for ballistic missile defense and offense. Prior to his association with AERL, he served a two-year term as Scientific Advisor to the Air Force, which followed his pioneering development of ablation heat protection and magnetohydrodynamic electrical power generation at General Electric Space Sciences Laboratory. He is currently Editor-in-Chief of the *AIAA Journal*, recipient of the Arthur D. Fleming Award for outstanding government service, and the AIAA Thermophysics Award. He is a Fellow of AIAA.

Received June 18, 1984; presented as Paper 84-1817 at the AIAA 17th Fluid Dynamics, Plasmadynamics and Lasers Conference, Snowmass, CO, June 25-27, 1984; revision received Sept. 21, 1984.

those areas that can be predicted with confidence and those areas that cannot. It is not intended to be an exhaustive review of all of the work accomplished, but to survey the fundamentals (see Appendix) and the highlights for both imaging systems and lasers.

The aero-optical disturbances may occur at several regions along the beam path: 1) in the laser cavity (or camera/telescope); 2) in a curtain flow that separates the laser from the local ambient propagation path; 3) in a beam transport tube; 4) in the region between the end of the beam transport tube and the local environment, e.g., in the flowfield of a vehicle; and 5) in the atmosphere.

This paper will concentrate on regions 3 and 4. Regions 1 and 2 were recently surveyed by Fuhs,[3] and 5 is outside the scope of the present paper. The plan of the paper is to discuss briefly gas cavity effects and curtain flow, then the beam transport tube, and finally the aero-optical phenomena between the end of the beam transport tube and a flowing ambient.

The same optical phenomena apply to imaging or laser projection due to reciprocity of the direction of propagation. Supposing one wishes to image a point source through an optically inhomogeneous medium (see Fig. 1a). At the image plane there will be an angular distribution of the light energy gathered by the lens. On the other hand, suppose one is propagating a laser beam through the same inhomogeneous medium, as in Fig. 1b. The angular spread of energy is the same at the imaging plane and at the laser focal plane. The rays have the same phase error because they follow the same path, within the paraxial and isoplanatic approximations. This permits a large portion of the formalism of imaging theory to be applied directly to the laser projection (see Table 1).

For a random inhomogeneous medium, one can determine the time-average beam spread of a laser which corresponds to long exposure of an optical system, either cw or repetitively pulsed. The time-average beam spread may be split into two components: beam wander of the energy distribution centroid, and spreading of the image about the centroid. The latter corresponds to short exposures for imaging or pulses for laser projection. For short exposures or pulses, one can calculate the ensemble-average distribution about the centroid for a large group of images or pulses. This turns out to be a smooth distribution. But each short-exposure image has an intensity distribution that is not a smooth monotonic function; it has a random irradiance distribution. The random irradiance distribution occurs in laser projection at the focal plane. This problem has been treated for imaging in some detail; the maximum irradiance standard deviation is about 100% of the mean[4] for small apertures, and decreases for larger apertures. Similar results are observed for laser projection. For extremely short monochromatic exposures, it has been found[5] that the recorded image consists of a cloud of images, each of which is essentially diffraction-limited by the size and optical quality of the aperture. The requirements for monochromaticity and very short exposure limit the number of photons captured. The images overlap each other, with the highest density of images at the centroid. For laser projection, the requirement for monochromaticity is met. Then the focal plane consists of speckles whose size is determined by the optical quality of the laser beam and its optical path.

Table 1 Optical analogies

Imaging	Laser projection
Point source, image angular distribution	Focal plane angular energy distribution
Long exposure	Time average, either cw or repetitively pulsed
Short exposure	Single pulse
Beam wander	Motion of the centroid
Speckle	Speckle

There is an important aspect of aero-optics which is unlike atmospheric propagation, namely, the difference in transverse scale size of the refractive index fluctuation. In atmospheric optics, the fluctuation scale size is many times that of the aperture size, while in aero-optics the reverse usually occurs. Thus, the scaling of the phase distortion for turbulence in atmospheric optics is $C_n \sim \Delta n/\Lambda^{1/3}$, while for aero-optics it is not C_n but the factor $\Delta n\Lambda^{1/2}$ for random disturbances. Thus, although the formalism of atmospheric optics applies to aero-optics in many cases, the effects and analytical expressions which quantify them are very different.

This paper is organized as follows: Section II covers phenomena within gas cavities and the transition or curtain flow between the cavity and the beam transport tube. Section III describes techniques for conditioning the laser beam transport tube. Sections IV, V, and VI deal with the transition to the external environment, which can be, respectively, a boundary layer, a cavity, or a turret. Finally, Sec. VII enumerates future opportunities for further understanding and implementation.

II. Laser Cavity Aero-optics

The optical quality of the gas inside the cavity of a flowing gas laser must be equal to that of an optical system that has been polished to great precision,[3] e.g., the resulting wavefront distortions must be smaller than 1 wavelength. This precision had been achieved easily in low-density electric-discharge gas lasers because of the small number of atoms or molecules in the optical path (but rarely in liquid dye or solid-state lasers because of their high density and low conversion efficiency). For the first of the high-power lasers, the gasdynamic laser, it was initially believed that turbulence in the cavity could become a major obstacle to achieving excellent beam quality. Specifically, the best of low-turbulence wind tunnels (transonic) had achieved relative density fluctuations of about 10^{-3}; this is the higher bound for acceptability in a gas laser cavity of reasonable length as given by Eq. (A29) in the Appendix.

Gasdynamic Lasers

For gasdynamic lasers (GDL), the cavity turbulence per se did not turn out to be an important problem because of both the low density and low turbulence level in the cavity. However, the ordered disturbances were important. The flow in a CO_2 gasdynamic laser cavity must be supersonic to reduce the static temperature to about 300 K, thereby relaxing the lower laser state of CO_2. In addition, the upper laser state is frozen by having the expansion time much less than

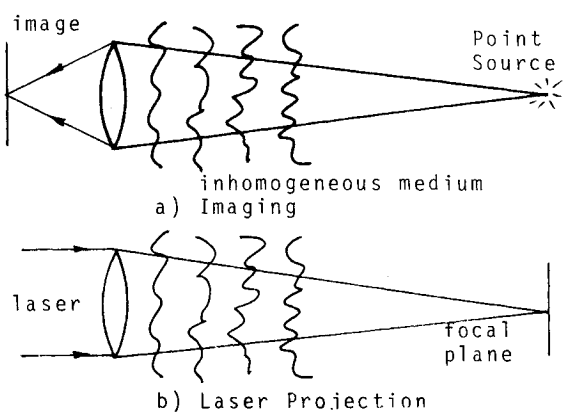

Fig. 1 Imaging and laser projection are reciprocal.

the vibrational relaxation time. To accomplish this very small (a fraction of a millimeter) nozzle throats are required. These conditions were met by making a row of precision two-dimensional nozzles in which the direction of expansion of the area is in the optical direction, with the nozzles affixed to the top and bottom of the cavity (see Fig. 2). This is quite different from the ordinary wind tunnel, in which one would carefully fair the nozzle throat walls into the top and bottom walls of the test section to avoid shock waves. The GDL arrangement caused shock waves from the ends of the nozzles on the top and bottom walls, as shown in Fig. 2, resulting from the interaction of the inviscid flow with the boundary layer.

The strengths of the shock waves were calculated[6] as well as measured interferometrically at the Avco Everett Research Laboratory.[7] These measurements indicated acceptable beam quality, using the "ordered" analysis of the Appendix. Unfortunately the on-axis intensity is a very strong function of the spatial rms phase error Φ; namely exp $(-\Phi^2)$, so that small errors in interpreting the interferograms led to large errors in the beam quality. This sensitivity to well-ordered inhomogeneities was greatly reduced by placing the optical path at an upstream-downstream angle relative to the optical path, as shown in Fig. 2, so that the rays crossed both shock and rarefaction waves. Thus, along the optical path, density increases were canceled by density decreases.

The specific performance of GDLs was improved by increasing the total gas temperature, which then required larger supersonic area ratios to maintain 300 K static temperature, which in turn required smaller throat areas. It became necessary to add spacer tabs in the nozzle blades to maintain the precision of the throat height. These tabs caused wakes; but canting the location of the tabs on the nozzle blades relative to the optical path alleviated this potential cause of disturbances (see Fig. 3). The result is similar to tilting the optical path. Thus, the steady, ordered disturbances of CO_2 GDLs were treated satisfactorily.

Unsteady, ordered disturbances exist in GDLs where the high total temperatures have been obtained by combustion. Combustors are designed for turbulent mixing to decrease the time for the reactants to burn. This, in turn, creates a very high level of acoustic noise, which feeds through the nozzle into the cavity. The impact on the density uniformity in the cavity can be large enough to alter the cavity optical mode, at least for an unstable resonator, which changes the output coupling and causes a temporal variation of the laser output power.

Electric Lasers, cw and Pulsed

Medium inhomogeneities occur even in a laser whose input gas supply is temporally much smoother than a GDL.[8] The mechanism is an instability in the heat release due to the quantum inefficiency of lasing. When an excited molecule is emitted, it drops to the lower laser state and then is collisionally deactivated to the ground state. The energy of the latter appears as translational energy, e.g., temperature. Since the waste heat release is isopycnic, the pressure rises, and is subsequently relaxed to the initial value by an acoustic wave. This relaxation changes the density distribution in the cavity, which in turn alters the optical mode, thus modifying the spatial dependence of lasing—and the heat release. There is the potential for closed-loop phenomena which, under certain conditions, can become unstable. The problem, however, was cured with side-wall acoustic mufflers[8,9] once the interdependent phenomenology was recognized. The recognition came from motion picture interferometry with very short exposures. Most frames showed a jumble of strong acoustic waves. As the cavity pressure was reduced, the cavity became less unstable, and the frames showed a fairly good medium, except that the interference lines were spatially sinusoidal and temporally oscillated about the null position, with a frequency corresponding to a cavity transverse acoustic mode. The amplitude of these disturbances grew in time. An optical mode analysis indicated a very strong dependence of the cavity extraction efficiency (and hence waste heat deposition) on small changes in the cavity optical path distribution. This was finally extended to a time-dependent acoustic mode-resonator mode analysis[10] which explained the phenomena.

Repetitively pulsed lasers display both a phenomenon similar to the above and another one. The latter is that the acoustic waves caused by the near-instantaneous deposition of the waste heat of the pulse must be damped out by acoustic absorbers before the next pulse. The former is similar to the cw mode-medium interaction described above, except that it occurs during the pulse. For an unstable resonator, the stimulated emission is spatially nonuniform because of both the expansion of the feedback rays and the Fresnel zones caused by the edges of the feedback mirror. This causes nonuniform spatial waste heat release, which in turn causes density gradients to appear. These gradients are proportional to the second spatial derivative of the heating rate and the third power of time. For pulses very short compared to the appropriate acoustic transit time, this should not be a problem, but for pulses an order of magnitude longer, this could be serious.[11]

Cavity Flow Curtains

Between the laser cavity flow and the local quiescent air of the compartment or room in which the laser is housed, there is usually an air curtain. This is necessary even when optical transmission windows are used on the cavity, in order to keep the laser gases away from the windows (e.g., chemical lasers). The laser gas mixture will usually have an index of refraction that differs from ambient, and the width of the mixing zone will depend on the relative velocity between the cavity gas and the curtain gas. The simplest approach is to have the refractive index of the curtain gas match that of the ambient, and the velocity of the curtain match that of the cavity (see Fig. 4). In that way, the width of the (turbulent) mixing layer is minimized where there is an index mismatch,

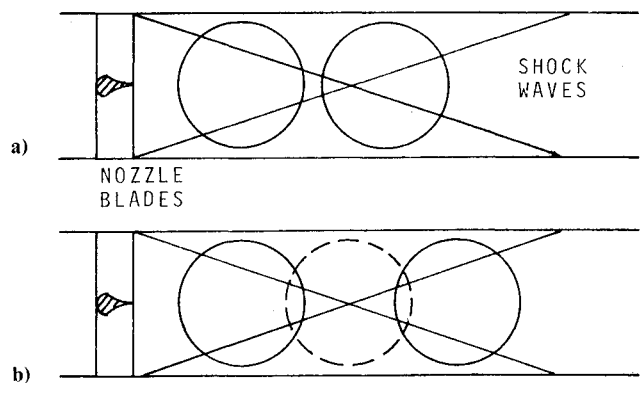

Fig. 2 Shock waves in a gasdynamic laser cavity: a) optical passes parallel to the shock waves, b) optical passes at an angle to the shock waves.

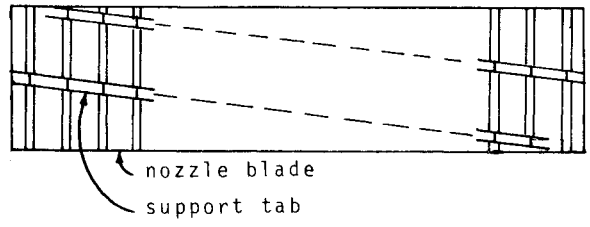

Fig. 3 Canted subsonic support tabs on gasdynamic nozzle blades.

and the effect of the velocity mismatch with similar indexes is also minimized. It was found that for the index mismatched layer, the rms index of refraction fluctuation is ~0.15 of the index of refraction difference.[12] This fractional value is consistent with the fluctuations of a passive scalar in a jet, which has a range of 0.13 to 0.2 of the difference of the maximum to minimum mean concentration. Supersonic aerodynamic windows have been surveyed elsewhere.[3]

III. Beam Transport Tube Conditioning

An interior optical path exists between the optical device and the external ambient environment. Because the environment in which the laser or passive optical imaging device is situated is often at a slightly different temperature than at the external ambient, density inhomogeneities can exist along the beam path. In addition, forced or natural convection in the internal environment caused by heat sources or sinks creates additional inhomogeneities. These are ameliorated by beam path conditioning, specifically a beam tube that isolates the beam path from the interior environment. For passive optics the main requirement is that the beam path be isothermal; often shutters are placed at the end(s) of the beam tube, which are only opened when the laser is in operation. For a laser, the beam tube can be filled with a nonabsorbing gas. If there are optics in the beam path that are heated by the laser or heated externally to prevent condensation, then the natural convection boundary layer over the surface can cause optical distortions. This can be removed using forced convection over the optical surface.

An alternate strategy is to use air as the beam tube medium, but air is slightly absorbing for many wavelengths due to the presence of nitrogen, water vapor, aerosols, and trace species. The absorbed energy then heats the air, causing optical distortions. The solution to avoid thermal blooming is to flow the air either transverse to the beam path or along the beam path. The former technique produces aberrations similar to those of atmospheric thermal blooming for rapid slewing. However, the axial flow technique has aero-optical effects caused by the turbulent transport of the absorbed energy to the beam tube walls. This effect was analyzed in Ref. 13 for a constant wall temperature, where it was shown that a temperature maximum was produced in the center of the tube. For long beam tubes in which inlet effects are small, the time-average optical distortion is obtained from the axisymmetric energy equation,

$$\rho C_p \frac{\epsilon_\theta}{r} \frac{\mathrm{d}}{\mathrm{d}r}\left(r\frac{\mathrm{d}T}{\mathrm{d}r}\right) = \alpha\left(\frac{P}{\pi R^2}\zeta - I(r)\right) \qquad (1)$$

where $\zeta = 1$ for insulated walls and 0 for constant wall temperature. P is the total power in the beam. The accuracy of Eq. (1) has been verified experimentally, for a TEM (10) radial intensity variation in Ref. 14, for various wall temperatures, using both Eq. (1) and a finite difference method for the entrance region. In both cases, ϵ_θ was taken as a function of position. A typical comparison is shown in Fig. 5. In actuality, the shape of the profile is predicted quite well by taking ϵ_θ equal to a constant.

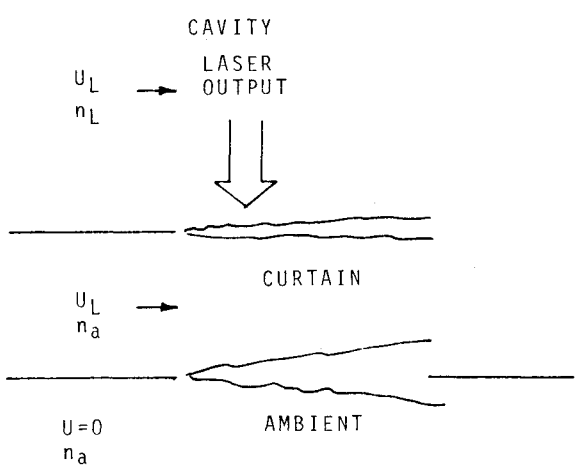

Fig. 4 Schematic of an optical curtain—L = laser, a = ambient.

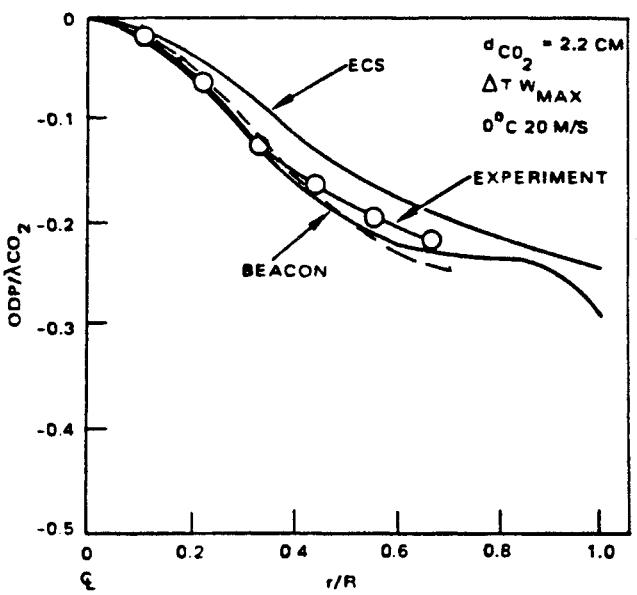

Fig. 5 Calculations and measurements of optical path wave-front distortion radial profile in units of 10.6 μm.[14] Beam profile was a modified Gaussian, $(1-2r^2/r_b^2)\exp(-r^2/r_b^2)$; $r_b/\sqrt{2}$ is nominal beam diameter. ECS is a radial integration with variable ϵ_θ, BEACON refers to a finite difference formulation,[14] and the dashed line is for ϵ_θ = const. The centerline-to-wall temperature difference was taken as zero.

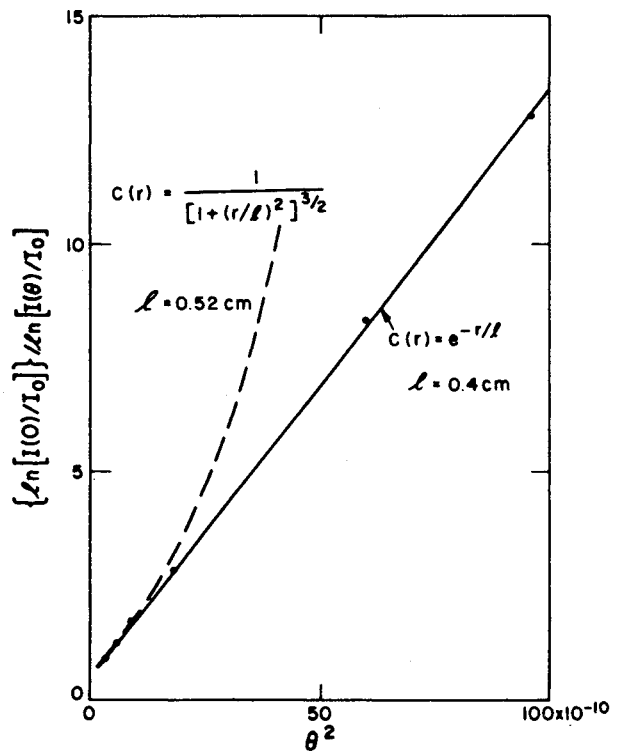

Fig. 6 Theoretical and experimental dependence of encircled power with aperture half-angle for two correlation functions for refractive index fluctuations.[15]

The optical distortion can be reduced by the following techniques:

1) Use of rough walls inside the beam tube to increase the turbulent mixing, at the expense of increased power to circulate the air.

2) Use of insulated walls, so that the centerline-to-wall temperature difference is minimized.

3) Use of heated walls, with a positive gradient in the flow direction to match the increase in temperature of the laser-heated air, which then further decreases the centerline-to-wall temperature difference.[14]

4) In Ref. 14, it was also suggested that swirl may be useful. A vortex may have a positive radial temperature gradient, while the thermal blooming causes a negative temperature gradient. However, the important parameter for the time-average ordered distortion is the mean radial density gradient. The density is inversely proportional to the temperature only in an isobaric situation. But for a vortex, the pressure gradient is always position, e.g.,

$$\frac{dp}{dr}=\rho\frac{v^2}{r}$$

Some typical cases are isothermal or adiabatic; the resulting density gradient in a vortex is

Isothermal

$$\rho(r)=\rho(0)\exp\left(\frac{\gamma-1}{\gamma}\int_0^r\frac{M^2}{r}dr\right) \tag{2}$$

Adiabatic

$$[\rho(r)]^{\gamma-1}=[\rho(0)]^{\gamma-1}+\int_0^r\frac{(\gamma-1)M^2}{r}dr \tag{3}$$

Thus, the radial density gradient is always positive; but that is precisely the same as for isobaric laser beam absorption. Thus, one may conclude that swirl does not compensate for the heating caused by laser beam absorption of the air in the beam transmission tube.

The above analysis was for the distortion caused by the radial density mean profile. But turbulence scattering will occur in accordance with Eq. (A29) since the flow is turbulent. For infrared wavelengths, this is negligible. For shorter wavelengths, the scattering is still small, but could be important. As an example, let the mean temperature difference be 1°C; the turbulent fluctuations will then be ~3% of that; assume a turbulence scale size of 1 cm, an index of refraction of air, and a wavelength of 500 nm (5000 Å). The resulting scattering is 0.23% per meter of path length. This is a negligible loss but could lead to heating of the walls or optics fixtures in the beam path.

The aero-optical phenomena due to flow of the ambient atmosphere beyond the beam tube are considered next.

IV. Boundary-Layer Flow

This and the next two sections are concerned with propagating the beam from the exit of the beam transport tube to the external ambient from an aircraft, through a turbulent boundary layer, a cavity, and a turret, respectively.

A turbulent boundary layer contributes considerable distortion due to two separate effects. The first is due to pressure fluctuations which vary as M^2; the second is due to temperature differences between the aircraft skin and the freestream. The latter is caused by temperature "recovery"; that is, the adiabatic aircraft skin temperature is greater than that of freestream;

$$\frac{T_w}{T_\infty}=1+R\left(\frac{\gamma-1}{2}\right)M^2 \tag{4}$$

where R is the recovery factor, which is close to unity. This creates a mean temperature gradient normal to the wall which is turbulently mixed and causes temperature and hence density fluctuations. Because both the pressure and temperature fluctuations vary as M^2, they are inseparable; hence they will be treated together. This appears to be the primary boundary-layer effect.

The basic theory of the angular distribution of scattered light is given in the Appendix. The unknowns are the spatial-average scale size of the turbulence and the magnitude of the fluctuations of the index of refraction. (The thickness of the turbulent boundary layer is known.) These unknowns were obtained by comparison[15] with experimental results. The experiment consisted of propagating an initially collimated light beam through a turbulent boundary layer normal to the surface and measuring the angular distribution of captured power through a series of different size apertures. For Eq. (A34), several elaborations are needed, as follows:

First, one may use an isotropic spectrum of turbulence, in which case $\theta=(\theta_x^2+\theta_y^2)^{1/2}$. There is little justification for this assumption, and several anisotropic spectra were tried,[15] but because the experimental apertures were circular, the anisotropic parameters are not separable. In any event, if circular distribution is desired, the isotropic assumption will have no effect on the results. Second, the general form of the spectrum used is

$$E_3=Fl^3(1+k_T^2l^2)^{-m} \tag{5}$$

where k_T is the spatial wave number of the turbulence and F is a constant, such that

$$\int_{-\infty}^{\infty}E_3(k)d^3k=1$$

The scattering coefficient per unit volume at angle θ then becomes

$$\sigma_s(\theta)\cong 2\pi k^4Fl^3(1+k^2l^2\theta^2)^{-m} \tag{6}$$

The total scattering coefficient for light out of a cone of half-angle θ is then

$$\sigma_T(\theta)=2\pi\int_\theta^\pi\sigma_s(\theta')\theta'd\theta'$$

and the light remaining in the cone of half-angle θ is given by

$$\frac{dI(\theta)}{dz}=-\sigma_T(\theta)I(\theta) \tag{7}$$

For averaged properties this becomes

$$\ell n\left(\frac{I(\theta)}{I_0}\right)=-\frac{2F\pi^2k^2\Delta n^2l\delta}{(m-1)(1+k^2l^2\theta^2)^{m-1}} \tag{8}$$

where I_0 is the incident intensity. The "on-axis" intensity $I(0)$ is obtained from Eq. (8) by letting $\theta\to 0$. The distribution of power through various apertures of half-angular divergence θ is then given by

$$k^2l^2\theta^2=\left\{\frac{\ell n[I(0)/I_0]}{\ell n[I(\theta)/I_0]}\right\}^{1/(m-1)} \tag{9}$$

There are three unknowns in Eq. (9): the turbulence scale size l, $I(0)$, and m. A value of m was assumed and the data $[\ell nI(\theta)/I_0]^{1/(m-1)}$ was plotted vs θ^2. If the correct value of m was chosen, the data should be a straight line; a value of $m=2$ provided the best fit, corresponding to an exponential correlation function. The ordinate intercept then gives

$I(0)/I_0$, which from Eq. (8) immediately gives Δn^2; while the slope is k^2l^2 (see Fig. 6). Since k is known, the turbulence scale size l is determined. Figure 7 gives the scale size, from which one can see that the scale size varies from ~0.16 to 0.1 of the boundary-layer height. Figure 8 gives the deduced density fluctuations as a function of various parameters. One may deduce that the rms density fluctuation is about 10% of the difference between the freestream density and the density near the (adiabatic) wall.

These results can be compared with wind tunnel hot-wire boundary-layer measurements which were interpreted as density fluctuations.[16] It was found that the density fluctuations, as a fraction of the wall-to-freestream density difference, were only 4-6% instead of about 10%. However, it is not clear that the wall temperature was adiabatic. In addition, the data reduction appeared to neglect the contribution of pressure fluctuations. On the other hand, the turbulent scale sizes in the flow direction and normal to the surface were found to be about 10% of the thickness of the turbulent boundary layer.

The use of porous boundary-layer fences was also investigated. Measurements in the same wind tunnel downstream of a porous fence whose height was less than the boundary-layer thickness indicated a factor of 3 increase in fluctuations. This occurred in a shear layer corresponding to the streamline from the edge of the fence, without substantial reduction of the fluctuations at other distances from the surface. Such fences upstream of windows also degraded the optical performance.[17] Early flight optical measurements on windows were made[18] using a shearing interferometer. It essentially measures the product of the aperture function and index of refraction disturbance in the integrand of Eq. (A31), except that the radial distance ρ is replaced by the direction of shear parallel to the surface. The turbulence parameters were determined by fitting the theoretical expression to the measurements. The resulting ratios of the scale sizes to boundary-layer thicknesses were 0.11 to 0.18, and density fluctuations were 0.11 to 0.21 of the density difference between freestream and wall. Considering the measurement spread, this can be considered as fair agreement.

Aerodynamic flight measurements[19] indicate that the longitudinal turbulence scale was about 0.2 and the normal turbulence scale size was about 0.1, respectively, of the turbulent boundary-layer thickness, as expected.

Later flight measurements were made using fine wire anemometer probes, a laser Doppler velocimeter, and a fast shearing interferometer. The flow instruments determined the boundary-layer profile of both the density fluctuations and the turbulence scale size, from which the theoretical extinction was determined by integration of Eq. (A30). This was compared to the optical extinction obtained by integration over the shear of the shearing interferometer output,[20] which is equivalent to setting $\theta = 0$ in Eq. (A31). As shown in Fig. 9, the resulting comparison is excellent. The measurements also confirmed that an exponential correlation function ($m = 2$) provided the best fit. More elaborate attempts at theoretical predictions, which are still based on empirically measured aerodynamic profiles, show much poorer agreement.[21]

To close this section, some calculated intensity profiles at the focus are shown in Fig. 10. Figure 11 shows the time-averaged on-axis intensity degradation as a function of boundary-layer thickness for some typical wavelengths and aircraft altitudes. It can be seen that for aircraft locations not too far rearward, little degradation is expected, even

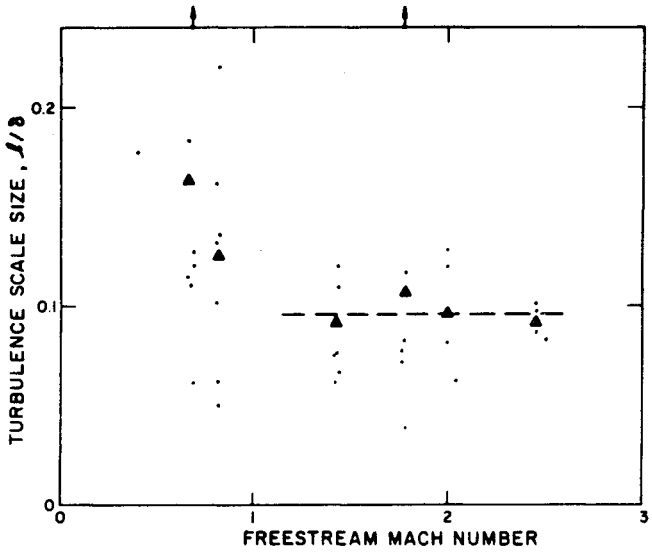

Fig. 7 Ratio of mass density fluctuation isotropic turbulence scale size to boundary-layer thickness.[15]

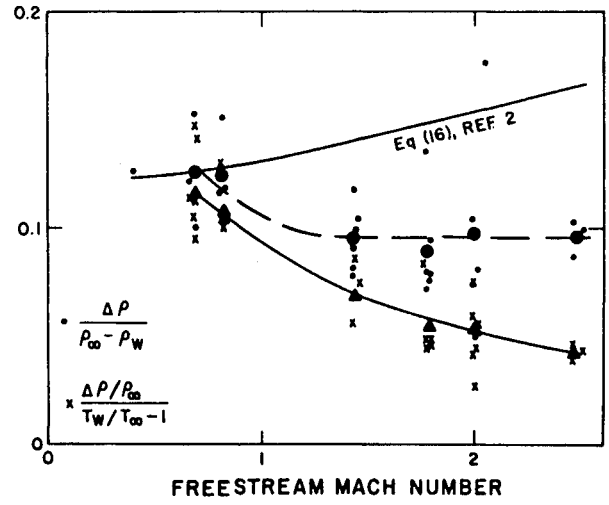

Fig. 8 Mass density fluctuation correlated to different parameters.[15]

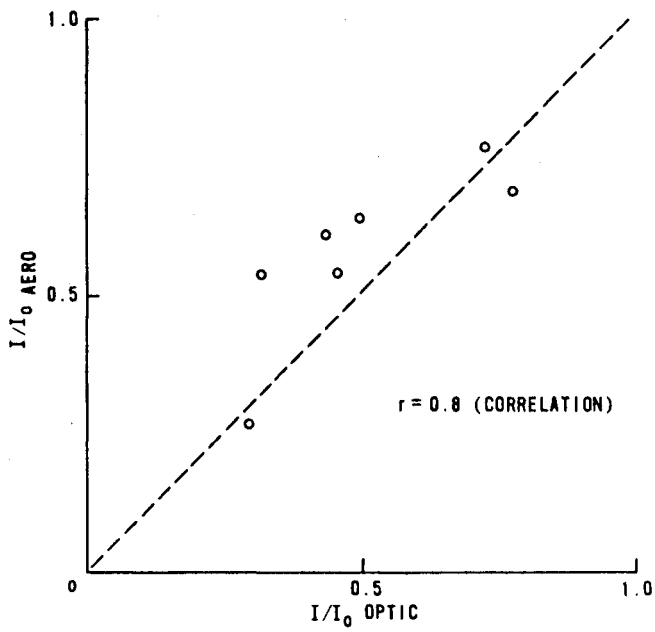

Fig. 9 Turbulent boundary-layer correlation plot. Ordinate is on-axis intensity deduced from boundary-layer measurements; abscissa is the same quantity as determined by integration of the output of a fast shearing interferometer.[20]

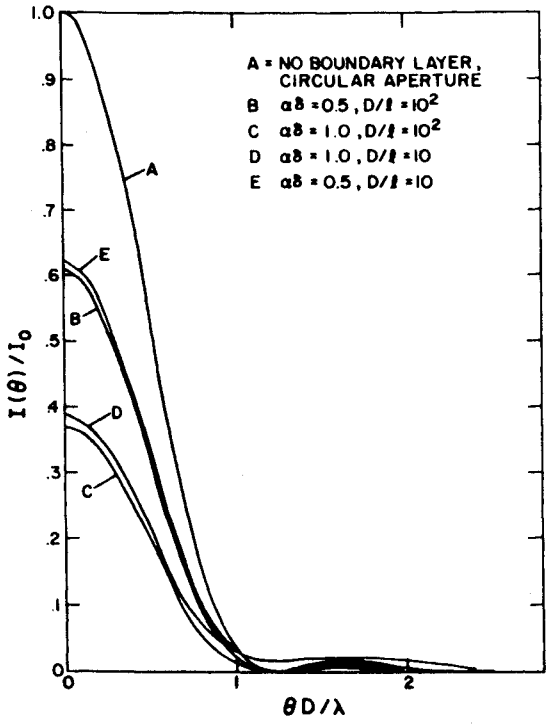

Fig. 10 Diffraction patterns from turbulent boundary layers.[15]

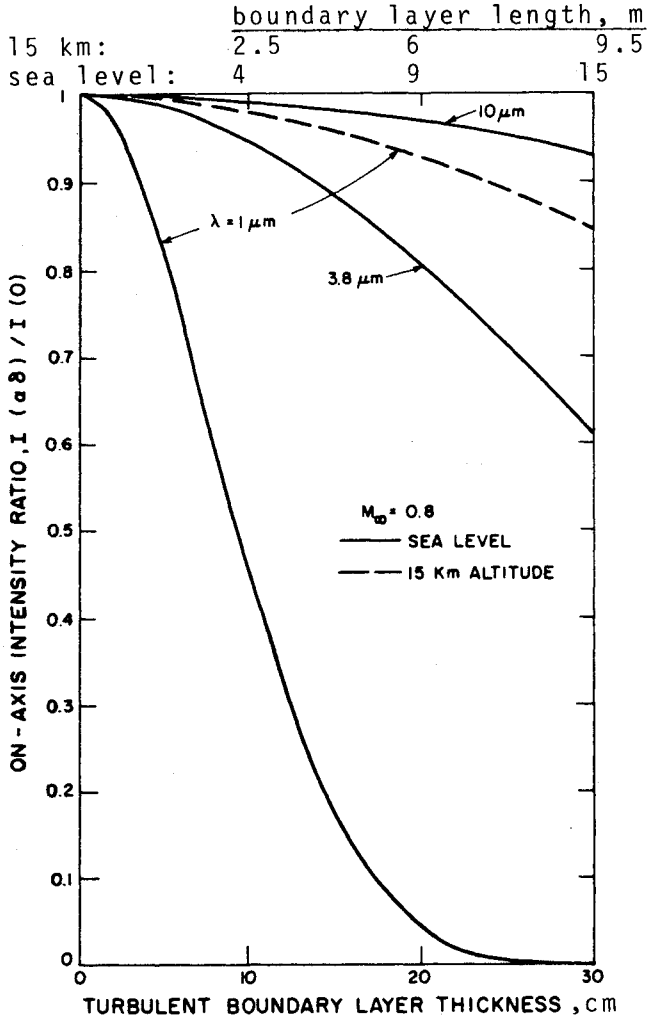

Fig. 11 Reduction of on-axis intensity for turbulent boundary layers.[15]

given the previous uncertainties in experimental measurements.

V. Cavity Aero-optics

The particular arrangement considered here is a cavity containing optics mounted flush with the fuselage of an aircraft. The flow in such a cavity will generally have a strong vortex within it and be unsteady unless it is correctly treated aerodynamically. To decrease the velocity that drives the vortex, porous boundary-layer fences have been tested. Wind tunnel tests, as indicated above, have shown that this caused a shear layer from the top of the fence with strong density fluctuations (three times that of a turbulent boundary layer).[16,21] These decreased as the fence height was decreased,[19] because the fence top was well inside the fuselage boundary layer. Measurements of optical quality in the same wind tunnel arrangement indicated that it improved[22] as the fence height was decreased, which is consistent with the aerodynamic measurement.

An example of such a fence arrangement on an aircraft is the NASA Kuiper Airborne Observatory, which is a C-141 with a 1-m-diam telescope.[23] Upstream of the cavity opening is an aerodynamic fence whose angle relative to the aircraft surface is adjustable from 0 to 90 deg. Slightly better optical performance was obtained when the fence elevation angle of 30 deg (but no measurements were presented for 0 deg). The fence is about 0.635 cm thick and has a porosity of 38% consisting of about ~1-cm holes drilled normal to the surface. The telescope is well stabilized and is capable of tracking a star to about 1.4 μrad rms.[24]

The fence minimizes the pressure fluctuations in the cavity to about 0.04 dynamic pressures. If one interprets this in terms of density fluctuations, this amounts to about 1-wavelength optical path distortion in the visible portion of the spectrum. If this contributed only to tilt, e.g., one part of the cavity was $+1\lambda$ while the other was -1λ, the total displacement of the image at the focal plane would be 4λ, or about 1.2 μrad, which is comparable to the telescope jitter.

The theoretical image angular diameter of a point source corresponding to an encircled energy of 85% for $\lambda = 0.62$ μm is about 1.7 μrad. The measured static telescope optical performance is about 8 μrad. In-flight measurements of the 85% encircled energy stellar image size gives 50-60 μrad for wavelengths that range from 0.62 to 3.1 μm (for long exposures), e.g., the in-flight optical quality is about 30 times diffraction limited in the visible. The visible images themselves appeared "torn"; that is, they are not axially symmetric. Short (1-ms) exposures decrease the visible image size by 50%, but that may be an artifact of the film sensitivity. The use of a flat glass window inserted in the cavity, but below the surface of the aircraft skin, caused little improvement, probably due to a shear layer above the window.

One possible explanation for the poor performance of the cavity is that the fence, with its holes forming jets which point into the cavity, created a thick, turbulent shear layer. The optical properties of the shear layer have been analyzed[25] using the relations derived in the Appendix, namely, the normalized intensity angular distribution is given by

$$I(\theta) = e^{-\phi^2}(1 - e^{-\Phi^2/2\sigma_1^2}) + (1 - e^{-\Phi^2})(1 - e^{-\theta^2/2\sigma_2^2}) \qquad (10)$$

where Φ is the rms phase error of the wave front; σ_1 the per-axis angular standard deviation of the diffraction-limited light, $= \sqrt{2}\lambda/\pi D$; and σ_2 the angular standard deviation of the scattered light, $= \sqrt{\pi}\lambda/\Lambda$. Using $\Lambda \approx 1$ cm and $\Phi = \sqrt{2}$, the distribution of the encircled power

$$\int_0^{\theta} 2\pi I(\theta')\theta' \, d\theta'$$

agrees well with the measurements. For example, the 85% encircled energy diameter is about 40 μrad. However, the use of the above equation for the near infrared predicts much smaller angular diameters for the 85% energy-encircled area. In fact, one may infer from the insensitivity of the data to wavelength that the distortion is caused by refractive effects rather than diffractive effects, which indicates the presence of large-scale flowfield inhomogeneities.

In principle, open-cavity operation should be possible. The downstream edge of the cavity should be sufficiently bluff to provide the dividing streamline a stagnation region to achieve nonoscillatory attachment. There is then a compromise between the height of the fence which thickens the boundary layer and the dynamic pressure in the cavity associated with the recirculation in it.

VI. Turret Aero-optics

A more complex technique for interfacing either a laser or an imaging system with the environment is a turret. Generally a turret will provide greater flexibility in the pointing direction. A typical configuration is a right circular cylinder, normal to the aircraft skin, capped by a sphere. The cylinder rotates in azimuth, while the optical port rotates in elevation. Either open cavities or solid windows are possible. The previous section described the aero-optical phenomena associated with open cavities; hence, in this section only the case of a closed window is considered. This permits concentration on the external aerodynamics in the vicinity of the turret. The first phenomenon encountered is that of compressible flow about a bluff body. The flowfield will have a spatial pressure distribution, which causes a spatial density distribution. This density distribution in turn causes an optical path difference for the rays entering or leaving the turret. Theoretical analyses have been performed for a zero-length cylinder. The solution for flow over the sphere consists of a first-order solution and Rayleigh's second-order solution to obtain the flow potential[26]:

$$\phi = \phi + M_\infty^2 \phi_1 = U\left\{\left(r + \frac{R^3}{2r^2}\right)P_1 + M_\infty^2\left(\frac{R^3}{3r^2} - \frac{R^6}{5r^5} + \frac{R^9}{24r^8}\right)P_1 + \left(\frac{3R^3}{10r^2} + \frac{27R^5}{55r^4} - \frac{3R^6}{10r^5} + \frac{3R^9}{176r^8}\right)P_3\right\} \tag{11}$$

where P_i are the Legendre functions $P_1 = \cos\theta$, $P_3 = (5/2)\cos^3\theta - (3/2)\cos\theta$. The local velocity is obtained from the potential function as $[(\partial\phi/\partial r)^2 + (r^{-1}\partial\phi/\partial\theta)^2]^{1/2}$, and use of the isentropic relations gives the local density. The results obviously scale with the radius of the sphere R, with velocity U, and with freestream Mach number M_∞. Figure 12 shows some typical results for the calculated phase distortions in terms of wavelength, for a turret azimuth angle = 0 deg facing the flow, and an elevation angle of 54 deg. The situation becomes more complex for other azimuth angles because of flow separation and unsteadiness, discussed next.

Bluff bodies in subsonic flow also have flow separation and unsteady flow caused by vortex shedding. This unsteadiness propagates throughout the flowfield adjacent to the turret. In addition, the stagnation region can cause separation upstream on the base plane. The nonsteady flow has been modeled using a finite difference approach.[27] Figure 13 shows some unsteady density profiles in the plane of symmetry; note the complexity of the density distribution. Figure 14 also shows the fluctuating component of the density. These are much larger than those permitted in gas laser cavities, and can lead to degraded optical quality. Downstream splitters and/or fairings behind the turret do not appear to completely solve the problem of unsteady flow.[28]

Extensive flowfield and optical measurements around a turret have been made in a wind tunnel.[29] In addition to the flowfield unsteadiness, a separated free shear layer appears over the optical opening at an azimuthal angle greater than 100 deg, leaving a turbulent wake. The distorted length of the optical path increased considerably with azimuthal angle, reflecting this effect. The scale sizes associated with the randomness were measured both by hot-wire anemometry and holography. The latter measurements showed a much smaller scale size than the former. The fluctuation density distribution deduced from hot-wire measurements is shown in Fig. 15 for three azimuthal angles. The increase in thickness of the fluctuating shear layer with azimuthal angle is apparent. The contribution of these fluctuations to the optical distortion is shown in Fig. 16. The effect of seeing through a thicker shear layer with increasing azimuthal angle is clear.

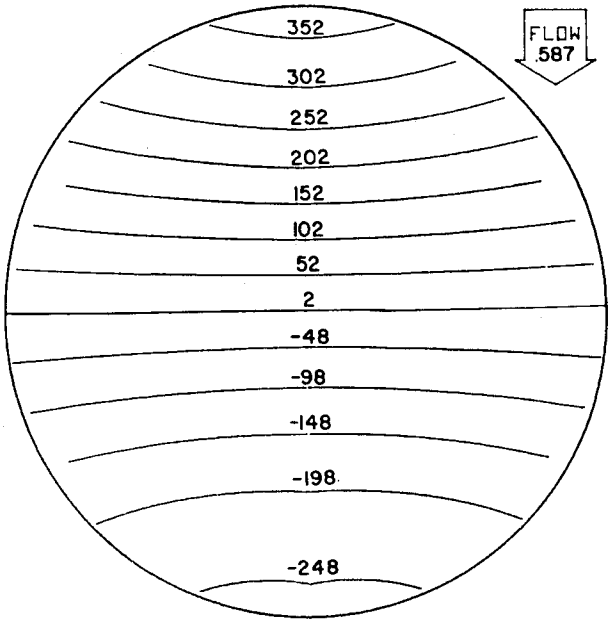

Fig. 12 Contours of constant wave-front distortion of 54-deg elevation angle, zero azimuth angle. $M = 0.587$, aperture diameter is 0.25 of the turret diameter of 0.914 m, and the wavelength is 3.8 μm. Contours are in terms of 10^{-2} wavelengths.[26]

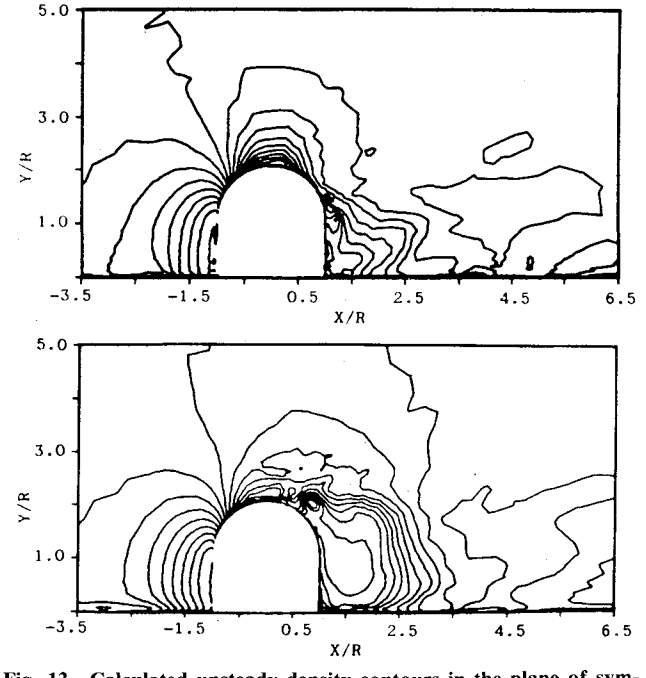

Fig. 13 Calculated unsteady density contours in the plane of symmetry of a turret.[27] $M = 0.55$, $Re = 10.3 \times 10^6$, and diameter = 0.44 m.

The scaling with Mach number is also clearly demonstrated, in that the distortion at $M=0.75$ should be about 80% greater than at $M=0.55$. These distortions are in addition to those of the ordered density disturbances in the mean flowfield surrounding the turret.

Although the optical distortions are potentially removable by very high spatial and temporal frequency phase conjugation, some noteworthy experiments have been performed to demonstrate that the flow separation could be removed by means of downstream suction.[30] In Ref. 30, a fairing was placed slightly downstream of the turret, with its upstream portion open and connected to suction blowers. The design criterion was that the suction speed at the nose piece be twice the freestream velocity. This resulted in the blower volumetric flow rate of about 36 m^3/s for a 0.427-m-diam turret at a freestream speed of 10 m/s. Two fairing nose pieces were tested: a uniform conformal nose piece and a tapered symmetric nose piece. The former required less volumetric flow rate. Figure 17 shows the position of flow tufts on the turret with and without suction. This clearly demonstrates that suction provides a technique for stabilizing the flow about a turret.

VII. Future Opportunities

With the future emphasis changing to visible and short wavelengths, aero-optics challenges will increase. In general the conditioning of laser cavity gas or telescope interiors will continue to be a challenge, but the theoretical basis and fundamental principles are well known. Careful application of those principles will be necessary. There are other potential means of correcting residual phase front errors, such as mechanical or optical phase compensation.

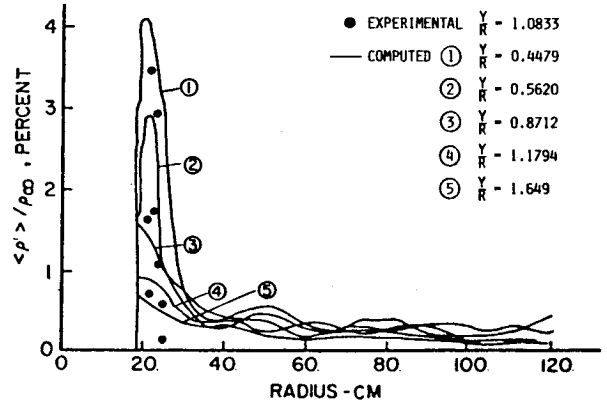

Fig. 14 Mass density rms fluctuations along a 90-deg ray.[27]

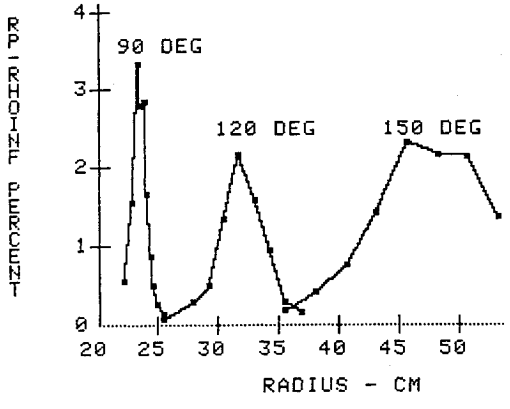

Fig. 15 Radial distribution of fluctuating mass density for $M=0.55$, for three azimuth angles.[29]

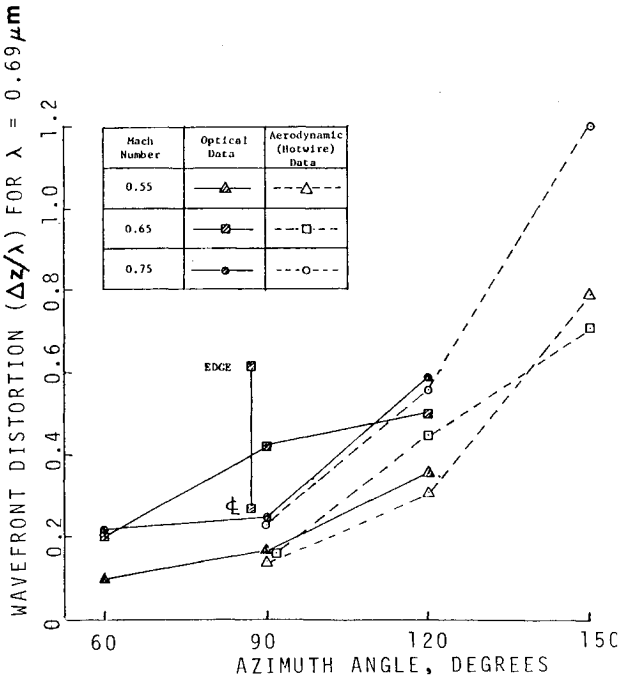

Fig. 16 Comparison of optically and aerodynamically deduced rms wave-front distortion.[29]

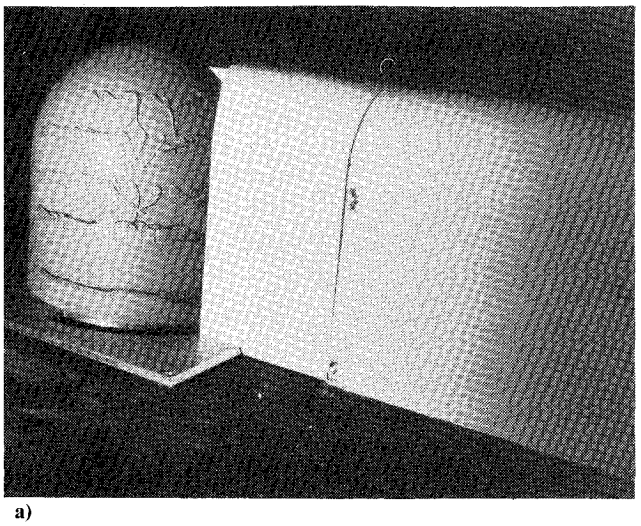

a)

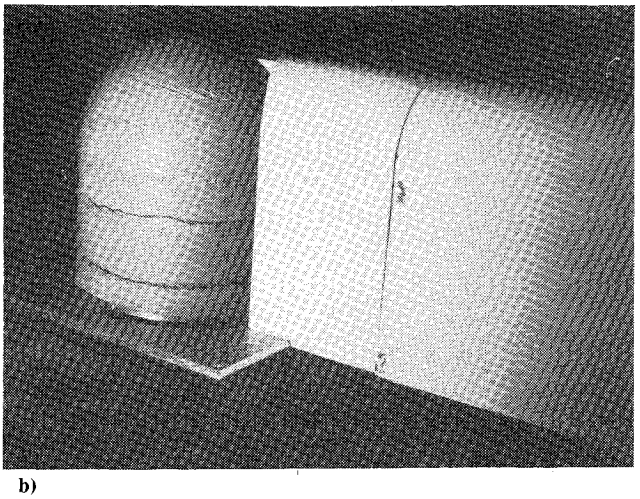

b)

Fig. 17 Demonstration of the effectiveness of suction flow control: a) flow control off, b) flow control on.[30]

The situation for airborne optics is less clear. In principle, a thin turbulent boundary layer should have negligible effect on short-wavelength propagation, as has been demonstrated both theoretically and in small-scale experiments. Full-size (1-m) optics have not yet been tried in flight with thin boundary layers.

For open-cavity optics the flight experiments of the Kuiper Airborne Observatory clearly indicate the opportunity for an order-of-magnitude improvement in optical quality by coupling more detailed diagnostics with configuration changes. These changes could include drilling the holes in the aerodynamic fence at the correct angle, reorienting the fence, and correct aerodynamic treatment of the downstream lip of the cavity.

Finally, for turret aero-optics, there seem to be only two choices: either use corrective phase conjugation optics with very high spatial and temporal frequencies, or use flow-separation control, for which there may be several possible techniques.[30] Even with separation control, a form of phase correction may still be needed to compensate for low spatial and temporal frequency distortions. Thus, the potential techniques for aircraft aero-optics applications, namely, boundary layers, open cavities, or turrets, all show promise, but none have been demonstrated full scale.

Appendix: Unified Theory of Diffraction Aberrations Caused by an Inhomogeneous Medium

Introduction

In the past, many specialized expressions have been derived and utilized in the area of diffraction aberrations caused by an inhomogeneous medium. This has encompassed both ordered and random distortions, with scale sizes both larger and smaller than the aperture diameter. In addition, various effects have been considered, including spreading of the intensity at the focal spot on a time-averaged basis and temporal intensity fluctuations at the focal plane. In the nomenclature of communication theory, the latter is known as fading. This Appendix will concentrate on the former aspect; the time-averaged intensity spreading at the focal spot. The basic starting point is Maxwell's equation:

$$\nabla \times \boldsymbol{E} = -\frac{\partial \boldsymbol{B}}{\partial t} \tag{A1}$$

$$\nabla \times \boldsymbol{H} = \frac{\partial \boldsymbol{D}}{\partial t} \tag{A2}$$

$$\boldsymbol{H} = \mu_0^{-1} \boldsymbol{B} \tag{A3}$$

for propagation in nonmagnetic media, and

$$\boldsymbol{D} = \kappa \boldsymbol{E} \tag{A4}$$

Substitution of Eqs. (A3) and (A4) into Eq. (A2) yields

$$\mu_0^{-1} \nabla \times \boldsymbol{B} = \frac{\partial \kappa \boldsymbol{E}}{\partial t} \tag{A5}$$

Taking the curl of Eq. (A1) and using Eq. (A5) yields

$$\nabla (\nabla \cdot \boldsymbol{E}) - \nabla^2 \boldsymbol{E} = -\mu_0 \kappa \frac{\partial^2 \boldsymbol{E}}{\partial t^2} \tag{A6}$$

The second term on the left side leads to a longitudinal component of the electric field which cancels the longitudinal component from the first term.[31] The final equation which describes the propagation is

$$\nabla^2 \boldsymbol{E} - \frac{n^2}{c_0^2} \frac{\partial^2 \boldsymbol{E}}{\partial t^2} = 0 \tag{A7}$$

where the index of refraction is given by $n = c_0/c$, the wavespeed $c = (\mu_0 \kappa)^{-1/2}$, and the vacuum wavespeed is given by $c_0 = (\mu_0 \kappa_0)^{-1/2}$. A typical technique for solving Eq. (A7) is a perturbation analysis, in which one takes $n = n_0 + n_1$; $\boldsymbol{E} = \boldsymbol{E}_0 + \boldsymbol{E}_1 + \ldots$, etc.[32] A more direct way is to neglect longitudinal higher derivatives of Eq. (A7) and obtain a direct solution of Eq. (A7).[33] These techniques, however, lead to a result that is equivalent to the following simple derivation.

We first model the propagation as a plane wave starting from $z = 0$ and propagating to $z = R$. We will deal with the angular dispersion; hence the analysis will apply to focused images as well. Finally, we make the scalar approximation $\boldsymbol{E} \equiv u$, and consider first vacuum propagation. Then Eq. (A7) becomes

$$\nabla^2 u = -c_0^{-2} \frac{\partial^2 u}{\partial t^2} \tag{A8}$$

For a periodic wave, $u \sim \exp(i\omega t)$, and with the wave number $k = \omega/c_0$, the solution to Eq. (A8) is

$$u(x_1, y_1, R) = -\frac{i}{\lambda} \int \frac{u_0(x,y,0) e^{ikr} \mathrm{d}A_0}{r} \tag{A9}$$

where A_0 is the aperture area, λ the wavelength, $u_0(x,y,0)$ the electric field at the aperture, $u(x_1, y_1, R)$ the electric field at $Z = R$ in the "focal" plane, and r the distance from $(x,y,0)$ to (x_1, y_1, R). Thus,

$$r = [(x_1 - x)^2 + (y_1 - y)^2 + z^2]^{1/2} \tag{A10}$$

With $R^2 = x_1^2 + y_1^2 + z^2$, Eq. (A9) becomes

$$r = R - \frac{x x_1}{R} - \frac{y y_1}{R}$$

We next convert to angles measured from the center of the aperture: $\theta_x = x_1/R$ and $\theta_y = y_1/R$. Then, noting that $\exp(ikr)$ varies much more rapidly than r^{-1}, Eq. (A10) becomes

$$u(\theta_x, \theta_y, R) = \frac{-i}{\lambda R} \exp(ikr) \times \int u_0(x,y,0) \exp[-ik(x\theta_x + y\theta_y)] \mathrm{d}A_0 \tag{A11}$$

If there is a phase distortion $\Phi(x,y)$ in the wave front at $z = 0$, then one multiplies the integrand of Eq. (A11) by $\exp(-i\Phi)$. The simplification added here is that the phase distortion is not (only) that at $z = 0$ but the cumulative phase distortion from $z = 0$ to R. This phase distortion is related to the wave-front distortion as $\Phi = 2\pi \Delta z/\lambda$ where Δz is the wave-front distortion,

$$\Delta z = z - z_0 \tag{A12}$$

This is related to the index of refraction variation as follows:

$$z = \int c \mathrm{d}t = c_0 \int n \mathrm{d}t = c_0 \int (n_0 + \Delta n) \mathrm{d}t = c_0 n_0 t + c_0 \int \Delta n \mathrm{d}t = z_0 + c_0 \int \Delta n \left(\frac{\mathrm{d}t}{\mathrm{d}z} \right) \mathrm{d}z \tag{A13}$$

or, with $c_0^{-1} \approx \mathrm{d}t/\mathrm{d}z$,

$$\Delta z = \int \Delta n(x,y,z) \mathrm{d}z \tag{A14}$$

here $\Delta n(x,y,z)$ is the index of refraction disturbance along a path from a point on the aperture to a point on the focal

plane. We may also neglect $\exp(ikR)$ because this term is canceled upon calculation of the intenstiy at the focal plane. The result is

$$\lambda(\theta_x,\theta_y)=\frac{-i}{\lambda R}\int u_0(x,y)\exp\left[ik\int_0^R \Delta n(x,y,z)\mathrm{d}z\right]$$
$$\times\exp[-ik(x\theta_x+y\theta_y)]\,\mathrm{d}x\mathrm{d}y \tag{A15}$$

Equation (A15) can be used for calculating the focal intensity for an ordered disturbance, even if time-dependent, or for a random inhomogeneous flow if the distribution of $\Delta n(x,t)$ is known. Computer models have been developed which do this by inserting phase screens between $Z=0$ and $Z=R$ and integrating Eq. (A9) from screen to screen.[34] However, Eq. (A15) can be integrated by recasting it in a manner that more typically describes random flow; that is, the variance of Δn and its spatial correlation function, as follows.

Random Medium

At the focal plane at angles (θ_x,θ_y), the intensity is the real product $u(\theta_x\theta_y)u^*(\theta_x,\theta_y)$, where both terms are the result of independent integrations over the aperture x,y. This is distinguished by using a prime on the second integration; thus:

$$I(\theta_x,\theta_y)\equiv uu^*=\frac{1}{\lambda^2R^2}\int\int\int\int u_0(x,y)u_0(x',y')$$
$$\times\exp\left\{ik\left[\int\Delta n(x,y,z)\mathrm{d}z-\int\Delta n(x',y',z')\mathrm{d}z'\right]\right\}$$
$$\times\exp[ik\theta_x(x'-x)]\exp[ik\theta_y(y'-y)]\,\mathrm{d}x'\mathrm{d}y'\mathrm{d}x\mathrm{d}y \tag{A16}$$

It is simpler to neglect the first exponential at first in order to simplify the quadruple integral of Eq. (A16). We thus hold x,y fixed and let $x'-x=\xi$, $y'-y=\eta$. Then Eq. (A16) becomes

$$I(\theta_x,\theta_y)=\frac{1}{\lambda^2R^2}\int\int\int\int u_0(x+\xi,y+\eta)$$
$$\times u_0(x,y)\exp[ik(\theta_x\xi+\theta_y\eta)]\,\mathrm{d}\xi\mathrm{d}\eta\mathrm{d}x\mathrm{d}y \tag{A17}$$

Next, integration is performed over (x,y). To simplify the result, we take $u_0=\text{const}$ for $x^2+y^2<D^2/4$, where D is the aperture diameter, and $u_0=0$ for $x^2+y^2>D^2/4$. Then, $u_0(x+\xi,\ y+\eta)$ is not constant over $x^2+y^2<D^2/4$, but instead is only finite over the common area of two circles spaced by $\rho\equiv\sqrt{\xi^2+\eta^2}$. This common area is given by

$$\tfrac{1}{2}(D^2\cos^{-1}(\rho/D)-\rho\sqrt{D^2-\rho^2}) \tag{A18}$$

Then, $\theta_x\xi+\theta_y\eta\equiv\boldsymbol{\theta}\cdot\boldsymbol{\rho}=\theta\rho\cos\phi$, where ϕ is the angle between $(i\theta_x+j\theta_y)$ and $(i\xi+j\eta)$. Finally, $\mathrm{d}\xi\mathrm{d}\eta$ can be expressed in cylindrical coordinates, $\rho\mathrm{d}\rho\mathrm{d}\phi$. Then Eq. (A17) becomes

$$I(\theta)=\frac{I_0}{2\lambda^2R^2}\int_0^D\int_0^{2\pi}\exp[ik\theta\rho\cos\phi]\,(D^2\cos^{-1}(\rho/D)$$
$$-\rho\sqrt{D^2-\rho^2})\rho\mathrm{d}\rho\mathrm{d}\phi \tag{A19}$$

where I is the focal plane intensity uu^* and I_0 is the aperture plane intensity u_0^2. Equation (A19) may be integrated to

$$I(\theta)=\frac{\pi I_0}{2\lambda^2R^2}\int_0^D\rho\mathrm{d}\rho J_0(k\theta\rho)\,[D^2\cos^{-1}(\rho/D)-\rho\sqrt{D^2-\rho^2}] \tag{A20}$$

Integration of Eq. (A20) gives rise to the usual Airy distribution of the intensity pattern,

$$I(\theta)=\frac{I_0D^2}{4R^2\theta^2}J_1^2\left(\frac{\pi D\theta}{\lambda}\right) \tag{A21}$$

In a similar manner, the effect of the random medium can be added. The term from Eq. (A16) is

$$\exp\{-ik[\textstyle\int\Delta n(x,y,z)\mathrm{d}z-\int\Delta n(x'+y'+z')\mathrm{d}z']\} \tag{A22}$$

To obtain the time-average intensity at the focal plane, the time average of expression (A22) is taken. For a Gaussian temporal distribution of the index of refraction fluctuations, Eq. (A22) becomes[35]:

$$\exp\{-\tfrac{1}{2}k^2\langle[\textstyle\int\Delta n(x,y,z)\mathrm{d}z-\int\Delta n(x',y',z')\mathrm{d}z']^2\rangle\} \tag{A23}$$

Consider one of the terms in expression (A23),

$$\int_0^R\int_0^R\langle\Delta n(x,y,z)\Delta n(x,y,z')\rangle\mathrm{d}z\mathrm{d}z' \tag{A24}$$

Holding z constant, and letting $z'=z+\zeta$, Eq. (A24) becomes

$$\int_0^R\mathrm{d}z\int_{z-R}^{z+R}\langle\Delta n(x,y,\zeta)\rangle\mathrm{d}\zeta \tag{A25}$$

For $R\gg\Lambda$ the integrand is the product of the mean-square index of refraction and the correlation function for the spatial distribution of inhomogeneities $C(\zeta)$. Further, if $\langle\Delta n^2\rangle$ does not vary greatly over a correlation length, then

$$\int_\theta^\infty\langle\Delta n^2\rangle C(\zeta)\mathrm{d}\zeta=\langle\Delta n^2\rangle(x,y,z)\Lambda(x,y,z) \tag{A26}$$

where Λ is the integral scale size of the random media. Similarly, the cross multiplication term becomes

$$\int_0^R\int_{z-R}^{z+R}\langle\Delta n^2(x,y,z)\rangle C(x,y,z;\ \xi,\eta,\zeta)\mathrm{d}\zeta\mathrm{d}z \tag{A27}$$

When $\Lambda\ll R$, the limits on ζ may be taken as $\pm\infty$; and with the use of Eqs. (A26) and (A27), Eq. (A23) becomes

$$\exp\left\{-2k^2\int_0^R\langle\Delta n^2\rangle(x,y,z)\left[\Lambda(x,y,z)\right.\right.$$
$$\left.\left.-\int_0^\infty C(x,y,z;\ \sqrt{\rho^2+\zeta^2})\mathrm{d}\zeta\right]\mathrm{d}z\right\} \tag{A28}$$

The first term in the exponential represents the scattering loss from the Airy diffraction pattern; one therefore arrives at the expression for the scattering coefficient α

$$\alpha=2k^2\langle\Delta n^2\rangle(x,y,z)\Lambda(x,y,z) \tag{A29}$$

Its integral is in fact the mean-square phase error $\langle\Phi^2\rangle$ along the path; hence, the loss is

$$\text{Loss factor}=\exp[-\langle\Phi^2\rangle]=\exp[-2k^2\textstyle\int\langle\Delta n^2\rangle\Lambda\mathrm{d}z] \tag{A30}$$

The phase error loss can be applied to either random or ordered media; however, in the case of the latter it is first necessary to subtract from the phase profile any tilt component $ax+by$; otherwise one is evaluating the intensity on one of the wings of the far-field profile. It is also necessary to subtract out the correct paraboloidal component of the phase; otherwise one is evaluating the effect at a point forward of or behind the true focal point, e.g., the value of z

corresponding to maximum intensity. These are common errors in aero-optics evaluation. One must also take into account the ratio of Λ to the aperture size. If it is small, then Eq. (A30) applies. But, if $\Lambda \gg D$, then the mean-square phase error is *not* that seen by the aperture; it only sees a fraction of $\Delta\Phi$, roughly $\Delta\Phi D/\Lambda$. This is the case of atmospheric propagation[36] and is treated by the use of expression (A28) in Eq. (A20) because the limit of integration D correctly limits the phase integration over the aperture, or

$$I(\theta_x,\theta_y)=\frac{\pi I_0}{\lambda^2R^2}\int_0^D \rho\mathrm{d}\rho J_0(k\theta\rho)\,[D^2\cos^{-1}(\rho/D) - \rho\sqrt{D^2-\rho^2}\,]\exp\left\{-2k^2\int_0^R\langle\Delta n^2\rangle \times\left[1-\int_0^\infty C(\sqrt{\rho^2+\zeta^2})\right]\mathrm{d}\zeta\right\}\mathrm{d}z \tag{A31}$$

Equation (A31) is suitable for evaluation of aero-optical phenomena.[37] It is also applicable for small scattering and atmospheric optics, treated below.

Small Scattering—Booker-Gordon Formulation

For small scattering $\alpha R \ll 1$, the second exponential can be expanded, and Eq. (A31) can be rewritten in Cartesian coordinates,

$$I(\theta_x,\theta_y)=\frac{I_0}{\lambda^2R^2}\iiiint\exp[ik\theta_x\xi]\times\exp[ik\theta_y\eta]\exp\left[-2k^2\int\langle\Delta n^2\rangle\Lambda\mathrm{d}z\right]\times\left[1-2k^2\int_0^R\int_0^\infty\Delta n^2C(\xi,\eta,\zeta)\mathrm{d}\zeta\mathrm{d}z\right]\mathrm{d}\xi\mathrm{d}\eta\mathrm{d}x\mathrm{d}y \tag{A32}$$

The first term is the extinction of the beam; the second term represents the scattered wave:

$$I_s(\theta_x,\theta_y)=\frac{I_0}{\lambda^2R^2}\exp(-\alpha R)\int_0^R\int_{-\infty}^\infty\exp[ik\theta_x\xi]\times\exp[ik\theta_y\eta]\langle\Delta n^2\rangle C(\rho)\mathrm{d}\rho\mathrm{d}r \tag{A33}$$

where $\rho=(\xi,\eta,\zeta)$ and $r=(x,y,z)$. Thus, $\mathrm{d}r=\mathrm{d}V$, an element of the scattering volume. Equation (A33) is multiplied by $\exp[ik\theta_z\zeta]$, where $\theta_z\equiv 0$. The integral over ρ is just the Fourier transform of the correlation function in which the spatial wave number becomes $k\theta$; thus,

$$I_s(\theta_x,\theta_y)=2\pi I_0k^4\exp(-\alpha R)\int_V\langle\Delta n^2\rangle 8\pi^3E_3\times(k\theta_x,k\theta_y,0)\mathrm{d}V \tag{A34}$$

where R is the range from the scattering volume, and E_3 is the three-dimensional spectrum of the index of refraction fluctuations. If E_3 is isotropic, it becomes $E_3(\theta)$, where $\theta=(\theta_x^2+\theta_y^2)^{1/2}$. For large angle scattering, θ is replaced by $2\sin(\theta/2)$, and a correction term $\cos\chi$ is needed to account for the angle χ between the incident electric field and the normal to the scattering direction.

Relation to Propagation Through Atmospheric Turbulence

The structure function of index of refraction fluctuations of Eq. (A23) can also be represented in terms of a structure function constant C_n:

$$\langle[\Delta n(x,y,z)-\Delta n(x',y',z)]^2\rangle=C_n^2\rho^{n-1} \tag{A35}$$

where $\rho^2=(x-x')^2+(y-y')^2$ for isotropic random inhomogeneities whose spatial spectrum $\sim k^{-n}$. For example, for fluid turbulence involving mixing of different temperatures or gases, $n=5/3$. However, there is a low value limit on k for this spectrum (the largest scale size), and a high value cutoff of k due to dissipation. These have no effect on these calculations as long as $k_{\text{low}}D\ll 1$, and $k_{\text{high}}D\gg 1$. Thus, the infinite spectrum k^{-n} can be used. The relation between the structure function and the correlation coefficient is

$$C(\xi)=1-C_n^2\xi^{n-1}/2\langle\Delta n^2\rangle \tag{A36}$$

Thus, the index of refraction structure function constant is approximately

$$C_n^2\sim\langle\Delta n^2\rangle/\Lambda^{n-1}$$

The argument in expression (A23) then becomes

$$D_\phi=k^2\int_0^R C_n^2\mathrm{d}z\int_{-\infty}^\infty[(\xi^2+\eta^2+\zeta^2)^{(n-1)/2}-\zeta^{n-1}]\mathrm{d}\zeta \tag{A37}$$

Again, we let $\rho=\sqrt{\xi^2+\eta^2}$ be the coordinate in the ξ,η plane. Then, noting that

$$(n-1)\int_0^\rho\rho'(\rho'^2+\zeta^2)^{(n-3)/2}\mathrm{d}\rho'=(\rho^2+\zeta^2)^{(n-1)/2}-\zeta^{n-1} \tag{A38}$$

the inner integral in Eq. (A37) becomes

$$(n-1)\frac{\rho^n}{n}\int_0^\infty\frac{\mathrm{d}\gamma}{\alpha^{1/2}(1+\gamma)^{(3-n)/2}}=\frac{(n-1)\rho^n}{n}\,\frac{\pi^{1/2}\Gamma(1-n/2)}{\Gamma((3-n)/2)} \tag{A39}$$

Finally,

$$D_\Phi=\frac{(n-1)k^2\pi^{1/2}\Gamma(1-n/2)}{n\Gamma((3-n)/2)}\rho^n(0)\times\int_0^L\left(\frac{\rho}{\rho_A}\right)^nC_n^2(z)\mathrm{d}z=A\rho(0)^n \tag{A40}$$

where $\rho(0)$ is the coordinate in the aperture plane. For a focused beam $\rho/\rho_A=(1-z/R)$. The final result is obtained by combining Eq. (A20) with Eq. (A40):

$$\langle I(\theta)\rangle=\frac{\pi I_0}{\lambda^2R^2}\int_0^D\rho\mathrm{d}\rho J_0(k\theta\rho)\,[D^2\cos^{-1}\times(\rho/D)-\rho\sqrt{D^2-\rho^2}\,]e^{-\frac{1}{2}D_\Phi} \tag{A41}$$

For example, the on-axis intensity ($\theta=0$) for strong turbulence is obtained by letting $\rho/D\ll 1$. For that case, an aperture coherence length r_0 is defined such that, in analogy with a diffraction-limited situation,

$$\langle I(0)\rangle=\pi Pr_0^2/4\lambda^2R^2;\quad r_0\ll D \tag{A42}$$

Equating Eq. (A41) to Eq. (A42), and for constant aperture power $P=\pi D^2I_0/4$, the result for the aperture coherence length is

$$r_0=\frac{\sqrt{8}2^{1/n}\sqrt{\Gamma(2/n)}}{n^{1/2}A^{1/n}} \tag{A43}$$

For intermediate values of r_0, the effective aperture size may be approximated by the inverse rss of r_0 and D.

The above results for $I(\theta)$ are for time-averaged intensity and actually consist of two contributions: the "wander" of the intensity centroid around the mean direction, and the

spreading of the intensity around that centroid. For example, if one is performing short-exposure photography or is using a pulsed laser whose pulses are short compared to the time for the random medium to change, then one may be interested in the peak intensity value, even though off axis. This is given, to within 1%, by[38]

$$I_{\text{pulse}}(0) = I_{DL}\{1 + 6.362 \times 10^{-4} \exp[5.41(D/r_0)^{0.3033}]\}^{-1} \tag{A44}$$

for $D/r_0 \lesssim 20$.

References

[1]Otten, L. J., "Introduction to Section II," *Progress in Astronautics and Aeronautics: Aero-Optical Phenomena*, Vol. 80, edited by K. Gilbert and L. J. Otten, AIAA, New York, 1982, p. 248.

[2]Kelsall, D., "Optical Measurements of Degradation in Aircraft Boundary Layers," *Progress in Astronautics and Aeronautics: Aero-Optical Phenomena*, Vol. 80, edited by K. Gilbert and L. J. Otten, AIAA, New York, 1982, p. 289.

[3]Fuhs, A. E., "Overview of Aero-Optical Phenomena," *Wavefront Distortions in Power Optics*, Vol. 293, edited by A. E. Fuhs and S. E. Fuhs, Society of Photo-Optical Instrumentation Engineers, Bellingham, Wash., 1981, pp. 36-55.

[4]Tatarski, V. I., *Wave Propagation in a Turbulent Medium*, McGraw-Hill Book Co., New York, 1961, p. 228.

[5]Gezari, D., Labeyrie, A., and Stachnik, R., "R. V. Speckle Interferometry: Diffraction-Limited Measurements of Nine Stars with the 200-Inch Telescope," *Astronophysical Journal*, Vol. 173, No. 1, Pt. 2, 1972, pp. L-1 to L-5.

[6]Simon, J. A., "Decay of a Boundary Layer Induced Shock," *AIAA Journal*, Vol. 9, July 1971, pp. 1417-1419.

[7]Ahouse, D., Wallace, J., Parmentier, E. M., and Mattsson, A., "Medium Quality Considerations for High Power Gas-Dynamic Lasers," *DoD Proceedings of the 5th Conference on Laser Technology*, Vol. 1, April 1972.

[8]Kellen, P. F., Mattsson, A. C., Ahouse, D. R., and Yoder, M. J., "Beam Properties of a CO_2 Continuous-Wave Electric-Discharge Laser," *Optical Engineering*, Vol. 18, May-June 1979, pp. 340-344.

[9]Ahouse, D. R. et al., "Electro-dynamic Laser with Acoustic Absorbing Electrode," U.S. Patent 4,278,950, July 14, 1981.

[10]Korff, D., Glickler, S., Tekula, M., Flusberg, A., Ballantyne, A., and Duzy, C., "Mode-Medium Interactions," *SPIE Proceedings*, Vol. 293, Paper 19, 1981.

[11]Flusberg, A., Korff, D., Cronburg, T., and Theophanis, G., "Mode-Medium Instability in Pulsed CO_2 Lasers," *Proceedings of Lasers '83*, Society of Optical and Quantum Electronics.

[12]Vu, B. T., Sutton, G. W., Theophanis, G., and Limpaecher, R., "Laser Beam Degradation Through Optically Turbulent Mixing Layers," AIAA Paper 80-1414, 1980.

[13]Valley, G. C., Shen, P. I-W., and Kelly, R. E., "Thermal Blooming in Axial Pipe Flow," *Applied Optics*, Vol. 18, Aug. 1979, pp. 2728-2730.

[14]Shen, P. I-W., Iyer, P. A., Rosser, W. A. Jr., Kelly, R. E., and Carey, M., "Beam Tube Thermal Blooming Experiment and Analysis,"AFWL TR-81-T129, April 1981.

[15]Sutton, G. W., "Optical Imaging Through Aircraft Turbulent Boundary Layers," *Progress in Astronautics and Aeronautics: Aero-Optical Phenomena*, Vol. 80, edited by K. Gilbert and L. J. Otten, AIAA, New York, 1982, pp. 15-39.

[16]Rose, W. C., "Unsteady Density and Velocity Measurements in the 6×6 Ft. Wind Tunnel," *Progress in Astronautics and Aeronautics: Aero-Optical Phenomena*, Vol. 80, edited by K. Gilbert and L. J. Otten, AIAA, New York, 1982, pp. 218-232.

[17]Gilbert, K. G., "Lear Jet Boundary-Layer/Shear-Layer Propagation Measurements," *Progress in Astronautics and Aeronautics: Aero-Optical Phenomena*, Vol. 80, edited by K. Gilbert and L. J. Otten, AIAA, New York, 1982, pp. 249-260.

[18]Kelsall, D., "Optical Measurements of Degradation in Aircraft Boundary Layers," *Progress in Astronautics and Aeronautics: Aero-Optical Phenomena*, Vol. 80, edited by K. Gilbert and L. J. Otten, AIAA, New York, 1982, pp. 261-293.

[19]Rose, W. C., Johnson, D. A., and Otten, L. J., "Summary of ALL Cycle II.5 Aerodynamic Shear and Boundary Layer Measurements," *Progress in Astronautics and Aeronautics: Aero-Optical Phenomena*, Vol. 80, edited by K. Gilbert and L. J. Otten, AIAA, New York, 1982, pp. 294-305.

[20]Gilbert, K. W., "KC-135 Aero-Optical Turbulent Boundary Layer/Shear Experiments," *Progress in Astronautics and Aeronautics: Aero-Optical Phenomena*, Vol. 80, edited by K. Gilbert and L. J. Otten, AIAA, New York, 1982, pp. 306-324.

[21]Verhoff, A., "Prediction of Optical Propagation Losses Through Turbulent Boundary/Shear Layers," *Progress in Astronautics and Aeronautics: Aero-Optical Phenomena*, Vol. 80, edited by K. Gilbert and L. J. Otten, AIAA, New York, 1982, pp. 40-77.

[22]Bailey, W. H. Jr., "Line Spread Instrumentation for Propagation Measurements," *Progress in Astronautics and Aeronautics: Aero-Optical Phenomena*, Vol. 80, edited by K. Gilbert and L. J. Otten, AIAA, New York, 1982, pp. 189-199.

[23]Buell, D. A., "Airloads Near the Open Port of a One-Meter Airborne Telescope," AIAA Paper 75-71, 1975.

[24]Erickson, E. F., "Summary of Observations of Image Quality of the Kuiper Airborne Observatory Telescope," KAO Workshop, NASA Ames Research Center, Hampton, VA, June 1982.

[25]Hohlfield, R. G., Dunham, E. W., and Sutton, G. W., "Telescopic Imaging Through Aircraft Turbulent Boundary Layers," submitted for publication to the Astronomical Society of the Pacific.

[26]Fuhs, A. E. and Fuhs, S. E., "Optical Phase Distortion Due to Compressible Flow Over Laser Turrets," *Progress in Astronautics and Aeronautics: Aero-Optical Phenomena*, Vol. 80, edited by K. Gilbert and L. J. Otten, AIAA, New York, 1982, pp. 101-138.

[27]Purohit, S. C., Shang, J. W., and Hankey, W. L. Jr., "Numerical Simulation of Flow Around a Three-Dimensional Turret," *AIAA Journal*, Vol. 21, Nov. 1983, pp. 1533-1540.

[28]Otten, L. J. and Gilbert, K. G., "Inviscid Flowfield Effects: Experimental Results," *Progress in Astronautics and Aeronautics: Aero-Optical Phenomena*, Vol. 80, edited by K. Gilbert and L. J. Otten, AIAA, New York, 1982, pp. 233-241.

[29]Craig, J. E., Trolinger, J. D., and Rose, W. C., "Propagation Diagnostic Technique for Turbulent Transonic Flow," AIAA Paper 84-0104, Jan. 1984.

[30]Schonberger, J. R., Fuhs, A. E., and Mandigo, A. M., "Flow Control for an Airborne Laser Turret," *Journal of Aircraft*, Vol. 19, July 1982, pp. 531-537.

[31]Tatarski, V. I., *Wave Propagation in a Turbulent Medium*, McGraw-Hill Book Co., New York, 1961, p. 64.

[32]Tatarski, V. I., *Wave Propagation in a Turbulent Medium*, McGraw-Hill Book Co., New York, 1961, p. 61.

[33]Taylor, L. S., "Decay of Mutual Coherence in Turbulent Media," *Journal of the Optical Society of America*, Vol. 57, No. 3, March 1967, pp. 304-308.

[34]Hermann, J. and Elbum, M., "Uplink Propagation and Adaptive Optics," *Proceedings of the IEEE National Telecommunications Conference*, No. 30, 1980, p. 27.3.1.

[35]Larson, H. J. and Shubert, B. O., *Random Variables and Stochastic Processes*, John Wiley, New York, 1979, p. 350.

[36]Fried, D. L., "Resolution Through Inhomogeneous Media," *Journal of the Optical Society of America*, Vol. 56, Oct. 1966, pp. 1372-1379.

[37]Sutton, G. W., "Effect of Turbulent Fluctuations in an Optically Active Fluid Medium," *AIAA Journal*, Vol. 7, Sept. 1969, pp. 1737-1743.

[38]Sutton, G. W., "Ground to Satellite Laser Beam Irradiance Due to Diffraction, Turbulence and Adaptive Optics," *SPIE Conference Proceedings*, Vol. 195, 1979, pp. 135-141.